Highlights

- A cable-suspended robot is presented with a spatial purely translational motion.

- Several special architectures are identified with distinctive and useful features.

- The singularity-free/reachable/interference-free workspaces are analytically found.

- The theoretical findings are validated by experimental tests.

- The robot can perform dynamic trajectories outside the static equilibrium workspace.

Dynamically feasible motions of a class of purely-translational cable-suspended parallel robots

Giovanni Mottola[a,*], Clément Gosselin[b], Marco Carricato[a]

[a]*Department of Industrial Engineering, University of Bologna, 40126 Bologna, Italy*
[b]*Department of Mechanical Engineering, Université Laval, Québec, QC G1V 0A6, Canada*

Abstract

We consider dynamic motions of a spatial robot suspended by six cables, arranged so as to form three parallelograms. Each parallelogram is composed by two parallel cables sharing the same length. Due to this arrangement, the end-effector can only translate. The cables in each parallelogram can be actuated by one motor: only three motors are then required, which reduces the robot complexity and cost. This robot may perform pick-and-place operations over large workspaces. We find tight conditions for feasibility of dynamic trajectories for the general architecture, and also special conditions such that the robot is dynamically equivalent to a 3-cable robot with a point-mass end-effector: then, the feasibility conditions previously developed for the dynamic trajectories of 3-cable point-mass robots can be profitably reused for the present case. To practically realize such dynamic trajectories, we also analyze the reachable, singularity-free and interference-free workspace, finding analytical expressions of their loci. Finally, we perform experiments where the robot follows dynamic trajectories outside its static workspace, thus finding confirmation that the orientation remains approximately constant.

Keywords: Cable-driven parallel robots, cable-suspended robots, parallel robots, translational motion, dynamics, parallelograms.

1. Introduction

In cable-driven parallel robots (CDPRs), the end-effector (EE) is connected to the frame by a number of cables whose lengths can be controlled. Cable-suspended parallel robots (CSPRs) are special types of CDPRs where cables are kept in tension mainly by the gravity force pulling the EE down. Fully-constrained CSPRs employ as many cables as the number of degrees of freedom (DOF) of the EE. The robot studied in this paper falls under this category.

If a CSPR moves in quasi-static conditions, inertia forces can be neglected, and the EE must remain within its static equilibrium workspace (SEW), defined as the set of poses where static equilibrium is possible with positive tensions in all cables [1, 2]. Recently, researchers have studied how to take advantage of inertia forces to keep cables in tension as the robot moves beyond its SEW. Here, a first fundamental distinction should be made between *redundantly-actuated*, *fully-actuated* and *under-actuated* robots, having a number of actuators respectively greater than, equal to or smaller than the number of DOFs. Some of the first works about the dynamics of under-actuated robots studied *pendulum-like* planar robots performing point-to-point motions [3, 4]. Regarding fully-actuated CSPRs, previous works have defined periodic or point-to-point feasible motions for 3-DOF spatial point-mass robots [5–11]. More recently, 6-DOF robots (with a finite-size EE) performing dynamic motions in space were also considered [12, 13]. Finally, some authors considered redundantly-actuated robots [14]. This approach expands the workspace, and thus the potential applications, of such robots.

Many applications do not require a full control of the EE pose, but only of the EE position while its orientation remains constant. A possible architecture that achieves this objective is obtained by suspending the EE by six cables that are kept pairwise parallel and with the same length, in a parallelogram fashion: this way, the EE can be shown to have only translational DOFs. A CSPR based on such an architecture was first proposed in [15] for post-disaster rescue operations; in this article, the authors studied the robot kinematics, proposed a calibration approach, and found the robot SEW by a numerical approach. A similar concept was used in [16] for an over-constrained 12-cable robot for the construction sector, focusing on the workspace within which the robot can resist forces and moments of known magnitude with positive cable tensions (the so-called wrench-feasible workspace). This work was further developed in [17], by performing numerical simulations on the robot controller along several dynamic trajectories. An overconstrained architecture based on a similar

---

idea was presented in [18, 19], where six passive cables were used to control the EE rotation and three active cables to displace the EE from one point to a target one; in the above contributions, the authors also studied the application of a gripper on the EE. Translational CSPRs were also proposed for large-scale 3D printing [20], or to help people affected by motion disabilities to overcome architectural barriers [21]. Other authors presented overconstrained architectures for CDPRs still based on a parallelogram arrangement of cables, but with positive cable tensions being ensured by antagonistic additional cables [22–25] or antagonistic jacks [26–29].

In the current contribution, we consider a general spatial robot with a finite-size EE suspended by six cables that define three parallelograms, so that the EE orientation remains constant as the robot moves. The CSPRs presented in [15, 20, 30] can be seen as special cases of the general architecture studied here. Since cables have pairwise identical lengths, this architecture allows the robot to be controlled by three actuators, thus simplifying design and reducing cost. The goal of our work is to use inertial effects acting on the EE to help in keeping cables taut. In this way: (i) the robot is controlled by only six cables (which is the minimum number for a fully-constrained architecture, cf. [31]) and there is no need for external tensioning devices; (ii) the workspace that can be reached by the robot is expanded. In this perspective, we combine and extend previous works on translational cable robots and dynamically feasible trajectories: our interest was in applying the wealth of scientific works already available on 3-DOF point-mass robots [5–11] to robots still having 3 DOFs but with a finite-size EE, which is a more realistic model. As seen above, CSPRs of this kind having a parallelogram actuation have found applications in various fields, but the possibility of using dynamic motions was not considered. This can be helpful when the robot footprint is limited due to space reasons: while the SEW is constrained by said footprint, dynamic motions allow the EE to reach a much wider workspace. This can be useful for robots that have to perform pick-and-place operations over large workspaces, if the EE follows a point-to-point trajectory such as those presented in [5, 7], where each target point is reached with zero velocity (but nonzero acceleration). Also, dynamic motions can be used to recover a robot in case of a cable breakdown [32]; if a robot with parallelogram actuation having more than 6 cables, for instance those presented in [17, 21–25], undergoes a sudden cable break, it could be brought back to its safe post-failure workspace by using dynamic trajectories such as those presented here for a 6-cable robot. Finally, cable robots can also be used for entertainment, as suggested in [33] where a robotic rollercoaster was proposed having a capsule driven by 3 cables for passengers to ride in; a translational parallel robot performing dynamical trajectories could provide a entertaining ride while avoiding rotational motions that could cause discomfort to passengers in some cases.

After introducing the robot geometry in Sec. 2, we present the conditions for positive cable tensions under the assumption that the only forces acting on the EE (other than the cable tensions) are gravity and inertia; we also model the cables as massless and infinitely stiff straight line segments, while the EE is an ideal rigid body. In Sec. 3 we consider the most general architecture, while in Sec. 4 we find special conditions that allow the dynamic equations to be greatly simplified, thus leading to a virtual 3-cable robot with a point-mass EE that is dynamically equivalent to our original robot. By this result, the feasibility conditions for dynamic trajectories of 3-cable point-mass robots [9] can be fully reused here. A method to define purely-translational dynamic trajectories for a finite-size EE controlled by six cables was already presented in [13]: however, the architecture proposed in [13] does not take advantage of parallelogram actuation and, thus, requires six motors to be independently controlled. Under the conditions given in Sec. 4, the robot SEW can be analytically defined, and has a very simple representation (cf. [15, 16], where the SEW was only numerically found).

For dynamic trajectories to be actually feasible, active and passive constraint singularities must be avoided, and practical limits due to cables' finite lengths and their possible interference must be taken into account. The corresponding loci are analytically derived in Secs. 5 and 6, respectively.

Our theoretical findings were tested on a prototype and the experimental results are presented in Sec. 7. The conclusions in Sec. 8 highlight the advantages of the architecture studied in this paper and outline our future work on the topic.

2. Robot geometry

Consider a spatial robot whose EE is connected to the base by six cables whose lengths can be controlled. The ith cable ($i = 1, ..., 6$) exits from the frame at point A_i, and it is attached to the EE at point B_i (Fig. 1a). P is the EE centre of mass. $Oxyz$ is a fixed coordinate system, with the z-axis pointing upward in the vertical direction. If $\mathbf{a}_i = A_i - O$, $\mathbf{b}_i = B_i - P$, and $\mathbf{p} = P - O$, the ith cable length is $\rho_i = \|\mathbf{a}_i - \mathbf{p} - \mathbf{b}_i\|$ (for obvious practical reasons, we may assume $\rho_i > 0$), whereas the cable direction is given by the unit vector $\mathbf{e}_i = (\mathbf{a}_i - \mathbf{p} - \mathbf{b}_i)/\rho_i$.

Motors are controlled so that, at every instant, $\rho_1 = \rho_2$, $\rho_3 = \rho_4$, and $\rho_5 = \rho_6$. This allows the number of actuators to be reduced to three, since each motor can simultaneously actuate two cables. Furthermore, the fixed and mobile cable attachment points are placed so that: $\|\mathbf{a}_2 - \mathbf{a}_1\| = \|\mathbf{b}_2 - \mathbf{b}_1\|$, $\|\mathbf{a}_4 - \mathbf{a}_3\| = \|\mathbf{b}_4 - \mathbf{b}_3\|$, and $\|\mathbf{a}_6 - \mathbf{a}_5\| = \|\mathbf{b}_6 - \mathbf{b}_5\|$. Also, in the initial configuration, cables $1 - 2$, $3 - 4$ and $5 - 6$ are mounted in such a way that they are pairwise parallel, so that $\mathbf{e}_1 = \mathbf{e}_2$, $\mathbf{e}_3 = \mathbf{e}_4$, and $\mathbf{e}_5 = \mathbf{e}_6$. As a result, the EE is suspended by three planar parallelograms: $A_1B_1B_2A_2$, $A_3B_3B_4A_4$, and $A_5B_5B_6A_6$. As long as all cables are taut, the parallelogram formed by cables i and j prevents the EE rotation about the direction $\mathbf{n}_{ij}$ normal to the parallelogram plane Π_{ij}. If $\mathbf{n}_{12}$, $\mathbf{n}_{34}$ and $\mathbf{n}_{56}$ are linearly independent, all rotations are prevented, and the EE can only translate. Furthermore, all parallelograms remain planar for finite motions. This architecture is similar to that of the Delta robot [15, 34].

Figure 1: Left: a 6-cable CSPR with three translational DOFs. Right: The planar parallelogram formed by cables i and j.

Since the EE preserves its orientation throughout any non-singular motion, all vectors fixed to the EE, such as $\mathbf{b}_i$ ($i = 1, \ldots, 6$), are constant.

3. Kinetostatic model

The forces exerted by the parallel cables i and j on the EE are $\mathbf{F}_i = \tau_i \mathbf{e}_i$ and $\mathbf{F}_j = \tau_j \mathbf{e}_j = \tau_j \mathbf{e}_i$. The resultant force and the resultant moment about P are, respectively (Fig. 1b)

$$\mathbf{F}_{tot_{ij}} = \mathbf{F}_i + \mathbf{F}_j \qquad\qquad = \mathbf{e}_i(\tau_i + \tau_j) \tag{1a}$$

$$\mathbf{M}_{tot_{ij}} = \mathbf{b}_i \times \mathbf{F}_i + \mathbf{b}_j \times \mathbf{F}_j = (\tau_i \mathbf{b}_i + \tau_j \mathbf{b}_j) \times \mathbf{e}_i \tag{1b}$$

It can be easily shown that this system of two forces is equivalent to a single force $\mathbf{F}_{ij} = \mathbf{e}_i \tau_{tot,ij}$ applied in point B_{ij} whose position is given by $\mathbf{p} + \mathbf{b}_{ij}$, where $\tau_{tot,ij} = \tau_i + \tau_j$, and

$$\mathbf{b}_{ij} = \frac{\tau_i \mathbf{b}_i + \tau_j \mathbf{b}_j}{\tau_{tot,ij}} = \sigma_i \mathbf{b}_i + \sigma_j \mathbf{b}_j = \sigma_i \mathbf{b}_i + (1 - \sigma_i)\mathbf{b}_j \tag{2}$$

where σ_i, σ_j are the tension ratios[2] defined as

$$\sigma_i = \frac{\tau_i}{\tau_{tot,ij}}, \ \sigma_j = \frac{\tau_j}{\tau_{tot,ij}} = 1 - \sigma_i \tag{3}$$

By definition (2), B_{ij} lies on the line passing through B_i and B_j. B_{ij} coincides with one of the endpoints if either $\sigma_i = 0$ or $\sigma_i = 1$; from Eq. (3), this is equivalent to $\tau_i = 0$ or $\tau_j = 0$, respectively. If both cables are taut, then $0 \leq \tau_i, \tau_j \leq \tau_{tot,ij}$, so $0 \leq \sigma_i, \sigma_j \leq 1$ and, consequently, B_{ij} lies on the segment $\overline{B_i B_j}$.

If m is the EE mass, $\mathbf{g} = [0, 0, -g]^T$ is the gravitational acceleration, and no wrenches other than gravity and inertia act on the platform, the dynamic equilibrium of the robot yields

$$\sum_{i=1}^{6} \mathbf{e}_i \tau_i \qquad = m\ddot{\mathbf{p}} - m\mathbf{g} = -\mathbf{F}_e \tag{4a}$$

$$\sum_{i=1}^{6} \mathbf{b}_i \times \mathbf{e}_i \tau_i = \mathbf{0} \tag{4b}$$

where the sum of gravity and inertial effects, $\mathbf{F}_e = m(\mathbf{g} - \ddot{\mathbf{p}})$, does not contribute to the moment equilibrium around P. We thus have a linear system of six equations in six unknowns, i.e. the cable tensions $\tau_1, \ldots, \tau_6$. This system can be simplified

---

[2]The definitions in Eqs. (2) and (3) are not valid if $\tau_{tot,ij} = 0$; however, this means either that one of the tensions is negative (against the assumption of cables being taut) or that $\tau_i = \tau_j = 0$. In this case, the parallelogram is not constraining the rotation along direction $\mathbf{n}_{ij}$, and the robot can no longer be considered translational.

by replacing the two cable forces $\mathbf{F}_i$ and $\mathbf{F}_j$ in each parallelogram by their resultant force $\mathbf{F}_{ij} = \mathbf{F}_i + \mathbf{F}_j = \tau_{tot,ij}\mathbf{e}_i$ applied in point B_{ij}. The equilibrium equations can thus be written as

$$\mathbf{M}\boldsymbol{\tau}_{tot} = -\mathbf{W}_e \tag{5}$$

where $\boldsymbol{\tau}_{tot} = [\tau_1 + \tau_2, \tau_3 + \tau_4, \tau_5 + \tau_6]^T$ is the vector of *total* cable tensions, $\mathbf{W}_e = \left[\mathbf{F}_e^T, \mathbf{0}^T\right]^T$ is the total wrench on the EE, and $\mathbf{M}$ is the 6×3 matrix:

$$\mathbf{M} = \begin{bmatrix} \mathbf{e}_1 & \mathbf{e}_3 & \mathbf{e}_5 \\ \mathbf{b}_{12} \times \mathbf{e}_1 & \mathbf{b}_{34} \times \mathbf{e}_3 & \mathbf{b}_{56} \times \mathbf{e}_5 \end{bmatrix} = \begin{bmatrix} \mathbf{M}_{sup} \\ \mathbf{M}_{inf} \end{bmatrix} \tag{6}$$

Equation (5) again defines a system of six equations in six unknowns, in this case the components of $\boldsymbol{\tau}_{tot}$ and tension ratios σ_i's in position vectors $\mathbf{b}_{ij}$'s, but it is decoupled, as $\boldsymbol{\tau}_{tot}$ can be computed by the first three relations in Eq. (5), and subsequently $\mathbf{b}_{ij}$ can be derived from the remaining ones. Indeed, by inverting the upper 3×3 block of $\mathbf{M}$, we can find the total cable tensions as

$$\boldsymbol{\tau}_{tot} = -\mathbf{M}_{sup}^{-1}\mathbf{F}_e \tag{7}$$

Matrix $\mathbf{M}_{sup} = \begin{bmatrix} \mathbf{e}_1 & \mathbf{e}_3 & \mathbf{e}_5 \end{bmatrix}$ is invertible as long as vectors $\mathbf{e}_1$, $\mathbf{e}_3$ and $\mathbf{e}_5$ are linearly independent. In order to interpret this condition in a more intuitive way, we define the auxiliary point A_i^* ($i = 1, \ldots, 6$) in the fixed frame given by the position vector $\mathbf{a}_i^* = \mathbf{a}_i - \mathbf{b}_i$. We notice that, for two cables i and j in the same parallelogram, $\mathbf{a}_i^* = (\mathbf{a}_j - \mathbf{b}_j) + [(\mathbf{a}_i - \mathbf{a}_j) - (\mathbf{b}_i - \mathbf{b}_j)] = \mathbf{a}_j - \mathbf{b}_j = \mathbf{a}_j^*$, since $\mathbf{a}_i - \mathbf{a}_j = \mathbf{b}_i - \mathbf{b}_j$ (Fig. 1b). Accordingly, we let $A_{ij}^* = A_i^* = A_j^*$ and $\mathbf{a}_{ij}^* = \mathbf{a}_i^* = \mathbf{a}_j^*$. The locations of points A_{ij}^*'s do not depend on the robot pose, since $\mathbf{a}_i$ and $\mathbf{b}_i$ are constant. By expressing the ith-cable direction as $\mathbf{e}_i = \left(\mathbf{a}_{ij}^* - \mathbf{p}\right)/\|\mathbf{a}_{ij}^* - \mathbf{p}\| = \mathbf{e}_j$, we see that $\mathbf{M}_{sup}$ is singular if and only if points P, A_{12}^*, A_{34}^* and A_{56}^* are coplanar. A special case of this condition occurs when points A_{ij}^*'s are collinear. If we exclude this degenerate architecture (which can be easily avoided at the design stage), we can define a singularity plane Π passing through points A_{12}^*, A_{34}^* and A_{56}^*. If P is not on Π, $\mathbf{M}_{sup}$ is invertible, and $\boldsymbol{\tau}_{tot}$ is given by Eq. (7).

We can now consider an *equivalent* robot with a point-mass EE controlled by three *virtual* cables passing through the auxiliary points A_{ij}^*'s. The cable tensions in the equivalent robot equal the total tensions $\tau_{tot,ij}$ in the original robot. If $\succeq$ denotes component-wise inequality, we must have

$$\boldsymbol{\tau}_{tot} \succeq \mathbf{0} \tag{8}$$

otherwise cable tensions in our translational CSPR cannot be all positive. The conditions for $\boldsymbol{\tau}_{tot}$ to be component-wise positive are the same as those presented in [9] for a point-mass EE suspended by three cables, namely,

$$\mu_{ij} := \left[\mathbf{p} \times (\mathbf{a}_{mn} - \mathbf{a}_{kl}) + \mathbf{a}_{mn} \times \mathbf{a}_{kl}\right]^T (\ddot{\mathbf{p}} - \mathbf{g}) > 0 \tag{9}$$

where indices k, l, m and n depend on indices i and j as follows:

$$\begin{cases} i = 1, j = 2 \rightarrow k = 5, l = 6, m = 3, n = 4 \\ i = 3, j = 4 \rightarrow k = 1, l = 2, m = 5, n = 6 \\ i = 5, j = 6 \rightarrow k = 3, l = 4, m = 1, n = 2 \end{cases} \tag{10}$$

The points A_{12}^*, A_{34}^* and A_{56}^* must be numbered clockwise (when seen along the positive z direction) and P must remain below Π. For example, all periodic and transition trajectories from [9] and point-to-point motions from [5] can be re-used here, and the total tensions are guaranteed to be always positive.

Requiring $\boldsymbol{\tau}_{tot}$ to be component-wise positive is a necessary, but not sufficient condition to guarantee that cable tensions in our translational CSPR are positive, since we might have $\tau_{tot,ij} > 0$ with $\tau_i > 0$ and $\tau_j < 0$ (or vice versa). A second condition to satisfy emerges from the last three equations in Eq. (5), namely

$$(\mathbf{b}_{12} \times \mathbf{e}_1)\tau_{tot,12} + (\mathbf{b}_{34} \times \mathbf{e}_3)\tau_{tot,34} + (\mathbf{b}_{56} \times \mathbf{e}_5)\tau_{tot,56} = \mathbf{0} \tag{11}$$

By considering the expression of $\mathbf{b}_{ij}$ in Eq. (2), and defining vector $\mathbf{d}_{ij} = \mathbf{b}_i - \mathbf{b}_j$ (which is a constant for a given robot, Fig. 1b), we may re-write Eq. (11) as

$$\mathbf{A}\boldsymbol{\sigma}_{135} = -\mathbf{b}_{246} \tag{12}$$

where

$$\mathbf{A} = \begin{bmatrix} (\mathbf{d}_{12} \times \mathbf{e}_1)\tau_{tot,12} & (\mathbf{d}_{34} \times \mathbf{e}_3)\tau_{tot,34} & (\mathbf{d}_{56} \times \mathbf{e}_5)\tau_{tot,56} \end{bmatrix} \tag{13}$$

$$\boldsymbol{\sigma}_{135} = \begin{bmatrix} \sigma_1 & \sigma_3 & \sigma_5 \end{bmatrix}^T \tag{14}$$

and

$$\mathbf{b}_{246} = (\mathbf{b}_2 \times \mathbf{e}_1)\tau_{tot,12} + (\mathbf{b}_4 \times \mathbf{e}_3)\tau_{tot,34} + (\mathbf{b}_6 \times \mathbf{e}_5)\tau_{tot,56} \tag{15}$$
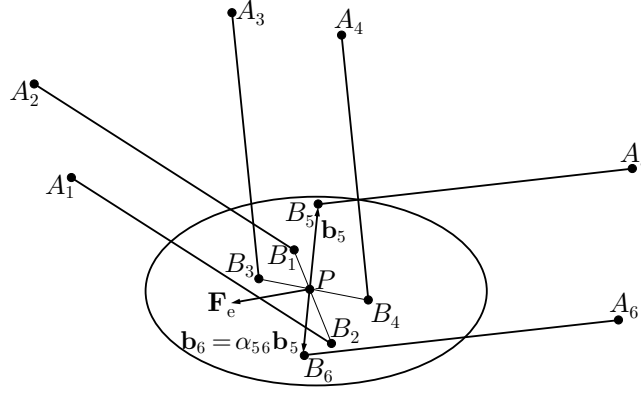
Figure 2: Schematic of the special architecture: the external force $\mathbf{F}_e$ acts on P, which is the intersection of segments $\overline{B_1 B_2}$, $\overline{B_3 B_4}$ and $\overline{B_5 B_6}$.

Equation (12) is a system of three equations in the unknowns $\sigma_1, \sigma_3, \sigma_5$, which can be solved once one knows the total tensions $\boldsymbol{\tau}_{tot}$. The second and final condition for positive tensions in all cables is, thus[3]:

$$\mathbf{0} \preceq \boldsymbol{\sigma}_{135} \preceq \mathbf{1} \tag{16}$$

Note that fulfilling Eqs. (8) and (16) only guarantees positive cable tensions, but this could be not sufficient: one may also require that a tension limit τ_{max} is not exceeded.

4. Special architecture

In this section we introduce a special robot architecture that allows us to define global conditions on a given trajectory so that condition (16) is always satisfied.

Let P lie at the intersection of lines $B_1 B_2$, $B_3 B_4$, and $B_5 B_6$ (Fig. 2). Vectors $\mathbf{b}_i$ and $\mathbf{b}_j$ are then aligned, so $\mathbf{b}_j = \alpha_{ij} \mathbf{b}_i$, where α_{ij} is a generic scalar, and thus $\mathbf{d}_{ij} = \mathbf{b}_i (1 - \alpha_{ij})$. Equation (12) becomes

$$\sum_{ij} (\mathbf{b}_i \times \mathbf{e}_i) \tau_{tot,ij} (1 - \alpha_{ij}) \sigma_i = -\sum_{ij} (\mathbf{b}_i \times \mathbf{e}_i) \tau_{tot,ij} \alpha_{ij} \tag{17}$$

where the indices in the summations on both sides take values $(i, j) \in \{(1, 2), (3, 4), (5, 6)\}$.

By comparing the left and the right hand side of Eq. (17), it can be seen that the equality always holds if $(1 - \alpha_{ij}) \sigma_i = -\alpha_{ij}$, namely

$$\boldsymbol{\sigma}_{135} = \begin{bmatrix} \frac{\alpha_{12}}{\alpha_{12}-1} & \frac{\alpha_{34}}{\alpha_{34}-1} & \frac{\alpha_{56}}{\alpha_{56}-1} \end{bmatrix}^T \tag{18}$$

Since the problem is linear, this is the only solution to Eq. (17), and it depends on neither the position $\mathbf{p}$ nor the external force $\mathbf{F}_e$.

It can be easily shown that the condition that we require for positive cable tensions, namely $0 \leq \sigma_i \leq 1$, becomes in this case $\alpha_{ij} \leq 0$. This in turn means that P, the centre of mass of the robot, must lie on segment $\overline{B_i B_j}$ *between* points B_i and B_j.

In summary, if:

- the three segments $\overline{B_1 B_2}$, $\overline{B_3 B_4}$, and $\overline{B_5 B_6}$ pass through a common point P,

- the resultant wrench $\mathbf{W}_e$ has zero moment about P (e.g., P is the centre of mass and $\mathbf{W}_e$ is only due to gravity and inertia),

---

[3] Note that we could also solve Eq. (11) for the other three tension ratios as

$$\mathbf{A} \boldsymbol{\sigma}_{246} = \mathbf{b}_{135}$$

with

$$\boldsymbol{\sigma}_{246} = \begin{bmatrix} \sigma_2 & \sigma_4 & \sigma_6 \end{bmatrix}^T$$

$$\mathbf{b}_{135} = (\mathbf{b}_1 \times \mathbf{e}_1) \tau_{tot,12} + (\mathbf{b}_3 \times \mathbf{e}_3) \tau_{tot,34} + (\mathbf{b}_5 \times \mathbf{e}_5) \tau_{tot,56}$$

In this case, condition (16) could equivalently be set as $\mathbf{0} \preceq \boldsymbol{\sigma}_{246} \preceq \mathbf{1}$.

then the tension ratios are constant, and in order to verify that cable tensions are positive we can simply check the total tensions $\tau_{tot,ij}$, namely condition (8).

It is worth observing that this result also leads to a very simple formulation of the static equilibrium workspace (SEW) for the robot at hand. Indeed, for the most general geometry of our translational robot, the SEW is the set of poses for which, when $\mathbf{F}_e = m\mathbf{g}$, $\boldsymbol{\tau}_{tot} \succeq \mathbf{0}$ (Eq. (8)) and $\mathbf{0} \preceq \boldsymbol{\sigma}_{135} \preceq \mathbf{1}$ (Eq. (16)). In general, these conditions define a complex volume in space: for instance, it may be proven that $\boldsymbol{\sigma}_{135} \succeq \mathbf{0}$ defines a 3rd-degree variety in x, y, z. However, for the special architecture introduced in this section, condition (16) is always satisfied, and only condition (8) must be checked. Due to the equivalence between this robot (with a finite-extension EE) and a 3-cable robot with a point-mass EE, we can immediately see that $\boldsymbol{\tau}_{tot} \succeq \mathbf{0}$ defines a vertical triangular prism having its upper vertices in A_{12}^*, A_{34}^* and A_{56}^* [35].

A particular design of the special architecture described in this section was proposed in [30]: in the latter article, P lies in the *middle* of the three segments $\overline{B_1 B_2}$, $\overline{B_3 B_4}$, and $\overline{B_5 B_6}$, so that $\alpha_{ij} = -1$ and $\boldsymbol{\sigma}_{135} = [1/2, 1/2, 1/2]^T$. Hence, the two cables in each parallelogram always have the same tension.

The result obtained in this section can also be compared with that found in [36] for a planar case, where the authors study a 3-cable planar CSPR with a finite-size EE, and with cables 2 and 3 defining a parallelogram, so that the EE motion is purely translational. The authors of [36] found that, if the applied forces (gravity and inertia) are applied in a point P lying on the segment through the attachment points of cables 2 and 3, and cable 1 is attached to P, this robot is dynamically equivalent to a 2-cable point-mass robot.

5. Singularities

We have seen in Section 3 that the robot reaches a singular configuration when matrix $\mathbf{M}_{sup}$ in Eq. (7) is not invertible and, thus, total cable tensions cannot be computed. This occurs when P lies on the plane Π defined by A_{12}^*, A_{34}^* and A_{56}^*. A second type of singularity emerges when tension ratios cannot be calculated, since matrix $\mathbf{A}$ in Eq. (12) is not of full rank. In both cases, matrix $\mathbf{M}$ in Eqs. (5)-(6) is undefined, since it comprises vectors $\mathbf{b}_{ij}$'s that depend on cable tensions τ_i's, which are undefined when the robot is at a singular configuration[4]. The union of the singularity loci of $\mathbf{M}_{sup}$ and $\mathbf{A}$ provides the complete singularity locus of the manipulator.

While the singularity given by $\det(\mathbf{M}_{sup}) = 0$ defines an *actuation singularity*, $\det(\mathbf{A}) = 0$ defines a *constraint singularity* [37, 38], since in the latter case the robot gains an additional freedom. Indeed, if $\mathbf{A}$ is re-written as

$$\mathbf{A} = \begin{bmatrix} \mathbf{c}_{12} & \mathbf{c}_{34} & \mathbf{c}_{56} \end{bmatrix} \tag{19}$$

with

$$\mathbf{c}_{ij} = (\mathbf{d}_{ij} \times \mathbf{e}_i)\tau_{tot,ij} \tag{20}$$

and in Eq. (8) the strict inequality holds (i.e. $\tau_{tot,ij} > 0$), $\mathbf{A}$ is singular when $\mathbf{c}_{12}$, $\mathbf{c}_{34}$ and $\mathbf{c}_{56}$ are coplanar (assuming $\|\mathbf{c}_{ij}\| \neq 0$; the special case $\|\mathbf{c}_{ij}\| = 0$ will be discussed later in this section). However, $\mathbf{c}_{ij}$ has the same direction as the vector $\mathbf{n}_{ij}$ orthogonal to the plane Π_{ij} through A_i, B_i, A_j and B_j (see Section 2), since $\mathbf{d}_{ij} \times \mathbf{e}_i$ is orthogonal to both $\mathbf{d}_{ij} = B_i - B_j$ and $\mathbf{e}_i$ (Fig. 1b). Therefore, if vectors $\mathbf{c}_{ij}$'s are coplanar, vectors $\mathbf{n}_{ij}$'s must be coplanar too: this is the condition where the robot is no longer purely translational and gains a rotational freedom.

The poses where $\mathbf{A}$ is singular are given by

$$\det(\mathbf{A}) = \frac{\tau_{tot,12}\tau_{tot,34}\tau_{tot,56}}{\rho_1\rho_3\rho_5} \left\{ [\mathbf{d}_{12} \times (\mathbf{a}_{12}^* - \mathbf{p})] \times [\mathbf{d}_{34} \times (\mathbf{a}_{34}^* - \mathbf{p})] \right\} \cdot [\mathbf{d}_{56} \times (\mathbf{a}_{56}^* - \mathbf{p})] = 0 \tag{21}$$

Since ρ_i and $\tau_{tot,ij}$ are nonzero, this reduces to finding the roots of the determinant of a matrix $\mathbf{A}'$ having column vectors $\mathbf{d}_{ij} \times (\mathbf{a}_{ij}^* - \mathbf{p})$ functions of position $\mathbf{p}$. After expanding and simplifying, this turns out to be a 2nd-degree variety in x, y, z, namely a quadric Σ.

In order to obtain an explicit formulation for Σ, we introduce some auxiliary parameters. First, we define the cross products

$$\boldsymbol{\lambda}_{ij,kl} = \mathbf{d}_{ij} \times \mathbf{d}_{kl} \tag{22a}$$

$$\boldsymbol{\lambda}_{a,ij} = \mathbf{d}_{ij} \times \mathbf{a}_{ij}^* \tag{22b}$$

where indices i, j, k and l range from 1 to 6, and pairs ij and kl denote two different parallelograms of the manipulator. We also define the cross products

$$\boldsymbol{\lambda}_{a,ij,kl} = \boldsymbol{\lambda}_{a,ij} \times \boldsymbol{\lambda}_{a,kl} \tag{23}$$

---

[4] This is equivalent to having the 6×6 coefficient matrix in the kinetostatic problem (4) to be singular.

and the two matrices

$$\boldsymbol{\Lambda} = \begin{bmatrix} \boldsymbol{\lambda}_{34,56} & \boldsymbol{\lambda}_{56,12} & \boldsymbol{\lambda}_{12,34} \end{bmatrix} \tag{24a}$$

$$\boldsymbol{\Lambda}_a = \begin{bmatrix} \boldsymbol{\lambda}_{a,12} & \boldsymbol{\lambda}_{a,34} & \boldsymbol{\lambda}_{a,56} \end{bmatrix} \tag{24b}$$

Since a general quadric in space can be expressed as

$$\mathbf{p}_e^T \mathbf{Q} \mathbf{p}_e = 0 \tag{25}$$

where $\mathbf{p}_e = [x, y, z, 1]^T$ and $\mathbf{Q}$ is a 4×4 matrix with real coefficients, it can be proven that the quadric defined by $\det(\mathbf{A}') = 0$ has

$$\mathbf{Q} = \begin{bmatrix} \mathbf{Q}_{3,3} & \mathbf{t} \\ \mathbf{t}^T & k_Q \end{bmatrix} \tag{26}$$

where the blocks composing $\mathbf{Q}$ are

$$\mathbf{Q}_{3,3} = -\frac{1}{2} \left[\boldsymbol{\Lambda}_a \boldsymbol{\Lambda}^T + \boldsymbol{\Lambda} \boldsymbol{\Lambda}_a^T \right] \tag{27a}$$

$$\mathbf{t} = -\frac{1}{2} \left[\mathbf{d}_{12} \times \boldsymbol{\lambda}_{a,34,56} + \mathbf{d}_{34} \times \boldsymbol{\lambda}_{a,56,12} + \mathbf{d}_{56} \times \boldsymbol{\lambda}_{a,12,34} \right] \tag{27b}$$

$$k_Q = -\boldsymbol{\lambda}_{a,12,34} \cdot \boldsymbol{\lambda}_{a,56} = -\boldsymbol{\lambda}_{a,34,56} \cdot \boldsymbol{\lambda}_{a,12} = -\boldsymbol{\lambda}_{a,56,12} \cdot \boldsymbol{\lambda}_{a,34} \tag{27c}$$

(the three definitions of k_Q are equivalent).

The full singularity locus for the manipulator is then given by $\det(\mathbf{M}_{sup}) \det(\mathbf{A}') = 0$, where $\det(\mathbf{M}_{sup}) = 0$ gives the plane Π and $\det(\mathbf{A}') = 0$ defines the quadric Σ. As a result, the singularity locus is given by a third-degree polynomial in x, y and z. This is coherent with the results reported in [39], where the authors found that the singularity locus of the general Gough-Stewart platform in the Cartesian space (for a given orientation of the platform) is a 3rd-degree polynomial in x, y and z. The manipulator at hand can be seen as a particular type of Gough-Stewart platform (assuming that all cables are taut and work as rigid legs) where the orientation of the EE is constant; the remarkable result is that the complex polynomial defined by Eq. (32) and Table 4 of the cited reference [39] can here be factored in two simpler terms of lower degree.

Analogous results were found for the 3-UPU translational manipulator in [40, 41], where the authors distinguished between translational and rotational singularities, showing that, for a specific architecture, the former define a plane and the latter define the union of a plane and a right cylinder. In [42], the author found the singularity locus for Delta-like translational manipulators of general architecture, but provided no explicit formulation as a function of the platform position. A rigid-link robot with three actuators and three translational DOFs, based on a parallelogram actuation system, was presented in [43]; our cable-driven architecture is conceptually similar. The singularity conditions of the robot in [43] were studied by assuming a symmetric architecture and by taking into account only the translational singularities: it can be shown that the singularity conditions provided in [43] correspond to the plane Π defined here. Another example can be found in [44], where the authors study a translational robot with three legs, and prove that the singularity surface is given by the union of a quadric and a plane (but in this case there are no constraint singularities, provided that some conditions on the robot architecture are fulfilled).

Fig. 3 qualitatively illustrates the singularity surface Σ for the robot at hand. Vector $\mathbf{n}_{34}$ (in green) is orthogonal to the plane Π_{34} passing through cables 3 and 4 (also in green). Idem for vectors $\mathbf{n}_{12}$ (in red) and $\mathbf{n}_{56}$ (in blue). Since $\mathbf{n}_{12}$, $\mathbf{n}_{34}$ and $\mathbf{n}_{56}$ are coplanar (i.e. they are parallel to plane Π_Σ), there is a direction, orthogonal to Π_Σ, around which the robot is free to rotate.

To help the reader visualize quadric Σ, we note that it has the following properties:

- It emerges from Eq. (21) that $\det(\mathbf{A}) = 0$ if $\mathbf{p}$ is equal to $\mathbf{a}_{12}^*$, $\mathbf{a}_{34}^*$ or $\mathbf{a}_{56}^*$. The three points A_{ij}^*'s are thus contained in Σ.

- Similarly, $\det(\mathbf{A}) = 0$ if $\mathbf{a}_{ij}^* - \mathbf{p}$ is aligned to $\mathbf{d}_{ij}$, so that the cross product of these two vectors is zero (this corresponds to the case $\|\mathbf{c}_{ij}\| = 0$). Thus, the line r_{ij} defined by $\mathbf{p} = \mathbf{a}_{ij}^* + \beta_{ij}\mathbf{d}_{ij}$, with $\beta_{ij} \in \mathbb{R}$, is contained in Σ; note that there are in fact three such lines, one for each parallelogram. It is known from projective geometry that there is one and only one quadric through a given set of three skew lines [45]; the quadric is then either a hyperbolic paraboloid (if the three vectors $\mathbf{d}_{ij}$ are all parallel to a single plane, but not to each other) or a hyperboloid of one sheet (otherwise). If instead the lines are not skew, the quadric could be a cylinder (either elliptic, parabolic or hyperbolic), a cone or the union of two planes (either parallel, intersecting or coincident). The possibility of the quadric being a cylinder can be ruled out by a geometric reasoning: if this were the case, the three lines r_{12}, r_{34} and r_{56} would be parallel, and so would be $\mathbf{d}_{12}$, $\mathbf{d}_{34}$ and $\mathbf{d}_{56}$. In this case the three vectors $\mathbf{n}_{12}$, $\mathbf{n}_{34}$ and $\mathbf{n}_{56}$ would have a common normal, and the robot would be architecturally singular. Accordingly, an architecture with all vectors $\mathbf{d}_{ij}$'s parallel is a degenerate case to be avoided. In a similar manner, it can be shown that Σ cannot be a cone: this could only happen if lines r_{ij} passed through a common point, but again, this would lead to a singular architecture.

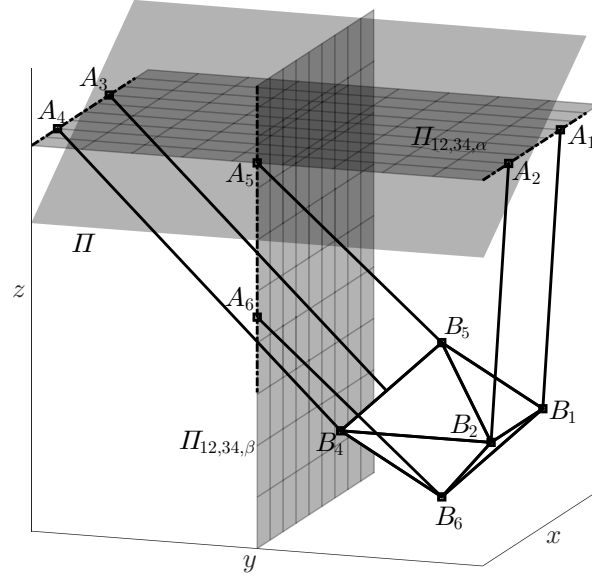We found two special architectures, described in the following, that lead to a simplified shape for Σ.

Figure 3: The singularity surface Σ for a translational cable-suspended robot with a general architecture.

5.1. Two spools are parallel

We first consider the case when vectors $\mathbf{d}_{ij}$ and $\mathbf{d}_{kl}$ are parallel, namely $\mathbf{d}_{ij} = f\mathbf{d}_{kl}$, $f \in \mathbb{R}$. Since $\mathbf{d}_{ij} = \mathbf{b}_i - \mathbf{b}_j = \mathbf{a}_i - \mathbf{a}_j$, this implies that segments $\overline{A_iA_j}$ and $\overline{A_kA_l}$ are parallel too. See Fig. 4 for an illustration of a possible implementation, where cables i and j (resp. k and l) in the same parallelogram are controlled by one spool rotating around an axis parallel to line A_iA_j (resp. A_kA_l).

If $\mathbf{d}_{ij} = f\mathbf{d}_{kl}$, the polynomial $\det[\mathbf{A}'(x, y, z)] = 0$ can be factored out in two linear terms, and surface Σ degenerates to the union of two planes $\Pi_{ij,kl,\alpha}$ and $\Pi_{ij,kl,\beta}$. These planes are generally unrelated to the plane Π defined by $\det(\mathbf{M}_{sup}) = 0$. It can also be proved that:

- Plane $\Pi_{ij,kl,\alpha}$ passes through points A_{ij}^* and A_{kl}^*, whereas $\Pi_{ij,kl,\beta}$ passes through point A_{mn}^*. Here, m and n are the indices of the two cables in the third parallelogram (in general, $\mathbf{d}_{mn}$ is parallel to neither $\mathbf{d}_{ij}$ nor $\mathbf{d}_{kl}$).

- Plane $\Pi_{ij,kl,\alpha}$ is orthogonal to vector $f\boldsymbol{\lambda}_{a,kl} - \boldsymbol{\lambda}_{a,ij}$, whereas plane $\Pi_{ij,kl,\beta}$ is orthogonal to both $\boldsymbol{\lambda}_{ij,mn}$ and $\boldsymbol{\lambda}_{kl,mn}$ (which are parallel in this case).

5.2. All spools are parallel to the same plane

Another case of practical interest is found when the three vectors $\mathbf{d}_{ij}$ are all parallel to the plane Π defined by A_{12}^*, A_{34}^* and A_{56}^*, as in Fig. 5. An example of such a robot is found in [30], where the authors show a design where all points A_i's are on the same horizontal plane Π, and all points B_i's are on the horizontal plane through P. Notice that, in the more general architecture illustrated in Fig. 5, neither points A_i's nor points B_i's are coplanar.

By choosing, without loss of generality, the fixed coordinate frame $Oxyz$ so that O lies in and z is normal to Π, the z components of both points A_{ij}^*'s and vectors $\mathbf{d}_{ij}$'s are all zero. With these simplifications, $\det(\mathbf{A}') = 0$ becomes

$$\det(\mathbf{A}') = -(\boldsymbol{\Lambda}\boldsymbol{\Lambda}_a^T)_{3,3}z^2 = 0 \tag{28}$$

where $(\cdot)_{3,3}$ denotes the 3rd element on the 3rd row of matrix $(\cdot)$. Clearly, Σ is in this case a degenerate quadric defined by two coincident planes with $z = 0$, so $\Sigma \equiv \Pi$.

6. Reachable workspace and cable interference

In order to be feasible, dynamic trajectories must satisfy, other than kinematic and kinetostatic constraints concerning cable tensionability and singularity avoidance, also physical constraints related to cable extension and interference. With regard to the former issue, the *reachable workspace* (RW) is the set of poses that can be reached with cable lengths comprised between a minimum and maximum value, that is, $\rho_i \in [\rho_{min}, \rho_{max}]$, $i = 1, \ldots, 6$. It can then be proved that point P must be comprised within two spheres, centred in A_{ij}^* and having radii ρ_{min} and ρ_{max}. The RW thus has spherical surfaces for boundaries: Fig. 6 shows the RW and the SEW for the robot used during the experiments described in Sec. 7.

Another issue to be considered is the possibility of cables interfering with each other, as this limits the workspace. The problem of defining the interference-free workspace of cable robots when the EE orientation is constant was studied

Figure 4: A simplified architecture, with the spools of cables $1-2$ and $3-4$ having parallel axes. The rotational singularity planes $\Pi_{ij,kl,\alpha}$ and $\Pi_{ij,kl,\beta}$ are shown with grid lines; the translational singularity plane Π is shown with no grid.
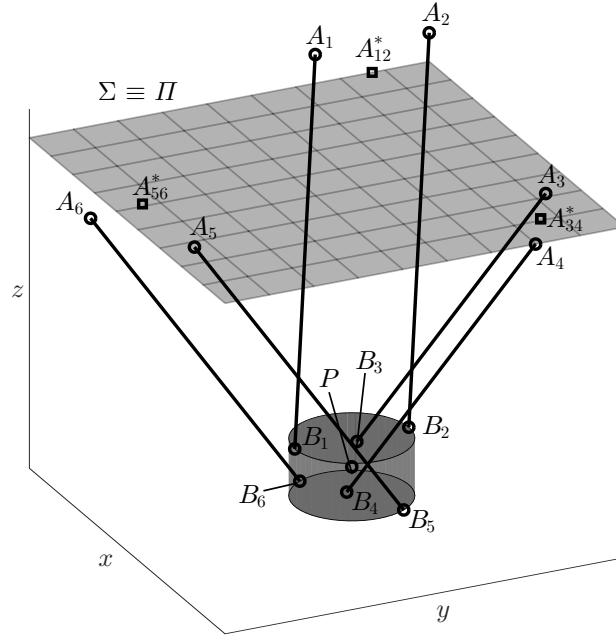

Figure 5: A simplified architecture with lines A_1A_2, A_3A_4 and A_5A_6 parallel to the plane Π through A_{12}^*, A_{34}^* and A_{56}^*.
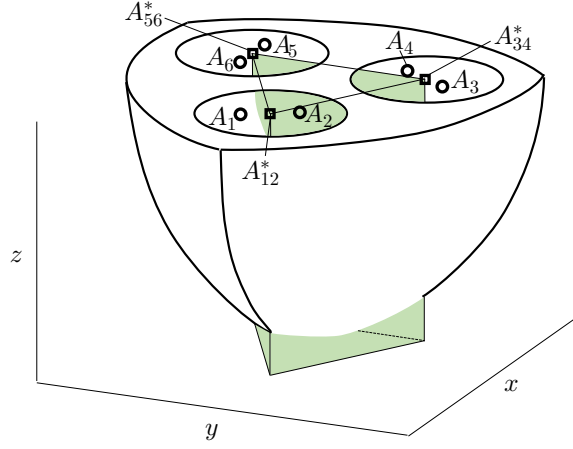
Figure 6: Static-equilibrium workspace and reachable workspace for the robot used in the experiments (Sec. 7). The SEW is a vertical triangular prism (in green) with upper vertices in points A^*_{12}, A^*_{34} and A^*_{56}. The RW is the volume (in white) comprised between three smaller spherical surfaces defined by $\rho_i = \rho_{min}$, three bigger spherical surfaces defined by $\rho_i = \rho_{max}$, and the plane Π passing through points A^*_{ij}.

in [46–48]. Two cables i and j in the same parallelogram are on parallel lines, so they can intersect only if the lines coincide: A_i, A_j, B_i and B_j must then be aligned, which is easily ruled out in practice. We thus consider two cables from different parallelograms: if they cross, they must be coplanar (this condition is necessary, but not sufficient, since cable lines might cross outside the cable span). In [47], it was shown that cables i and k are coplanar if and only if

$$(\Delta \mathbf{a}_{ki} \times \mathbf{d}_{ki}) \cdot (\mathbf{p} - \mathbf{a}_i + \mathbf{b}_i) = 0 \tag{29}$$

where $\Delta \mathbf{a}_{ki} = \mathbf{a}_k - \mathbf{a}_i$. Equation (29) holds in these cases:

a) $\Delta \mathbf{a}_{ki} = \mathbf{0}$ or $\mathbf{d}_{ki} = \mathbf{0}$, namely if $A_i = A_k$ (respectively $B_i = B_k$): the cables cross in $A_i = A_k$ (resp. $B_i = B_k$).

b) $\Delta \mathbf{a}_{ki}$ is parallel to $\mathbf{d}_{ki}$, so $\Delta \mathbf{a}_{ki} \times \mathbf{d}_{ki} = \mathbf{0}$: this is a special architecture in which cables i and k are always coplanar[5].

c) $\mathbf{p} - \mathbf{a}_i + \mathbf{b}_i = \mathbf{0}$: this can only happen if the i-th cable has zero length, since $\mathbf{p} - \mathbf{a}_i + \mathbf{b}_i$ is the vector from A_i to B_i.

d) $\Delta \mathbf{a}_{ki} \times \mathbf{d}_{ki}$ is orthogonal to $\mathbf{p} - \mathbf{a}_i + \mathbf{b}_i$, which is the general case considered in [47].

Excluding special cases a to c, Eq. (29) defines a plane Ω_{ik}: if $P \in \Omega_{ik}$, cables i and k are coplanar and thus can cross.

A special architecture can be usefully considered here, with all points A_i's lying on a plane Γ and all points B_i's lying on a plane parallel to Γ. In this case, the singularity plane Π through A^*_{12}, A^*_{34} and A^*_{56} is also parallel to Γ[6]: we are thus in a special case of the architecture seen in Subsection 5.2. It can then be seen that Ω_{ik} coincides with the singularity plane $\Pi \equiv \Sigma$. For a robot such as the one in [30], then, there can be no cable interference unless the robot is at a singular configuration. This makes such an architecture attractive as the singularity-free and the interference-free workspaces coincide and very simple to visualize: therefore, this architecture was used for our tests (see Section 7).

7. Experimental tests

In this section, we present the results of the tests performed on a prototype at Université Laval. The robot was designed so that the cable attachment points B_i's define a regular hexagon, with the centre of mass P in its centre. The cable exit points A_i's are placed on the sides of an equilateral triangle, as shown in Fig. 7a. The six cables are wound on three motorized winches, each moving two cables simultaneously. The winches are composed of two coaxial pulleys (both connected to a servomotor) of the same radius; the cables in each parallelogram wind simultaneously on different pulleys, in order to avoid interference between cables. In this way, if the pulley rotates by a given angle, the two cables wind on the pulleys by the same amount (since the winding radius is the same) and thus their lengths remain equal, provided that they were equal at the beginning of the motion. The motor axes pass through the auxiliary points A^*_{ij}'s, and in this case A_i and A_j are symmetrical with respect to A^*_{ij}. The location of the motors and the cable exit points was chosen so as to have a large workspace and avoid cable interference. The final prototype is shown in Fig. 7b and the winches are in Fig. 7c. The prototype is controlled via a Simulink model where the user can set the desired trajectory and its parameters; the platform coordinates in Cartesian space are converted in corresponding rotation angles in the joint space by the inverse kinematics. The motors' target positions are then sent to the real-time control system of the robot, based on a PID control loop.
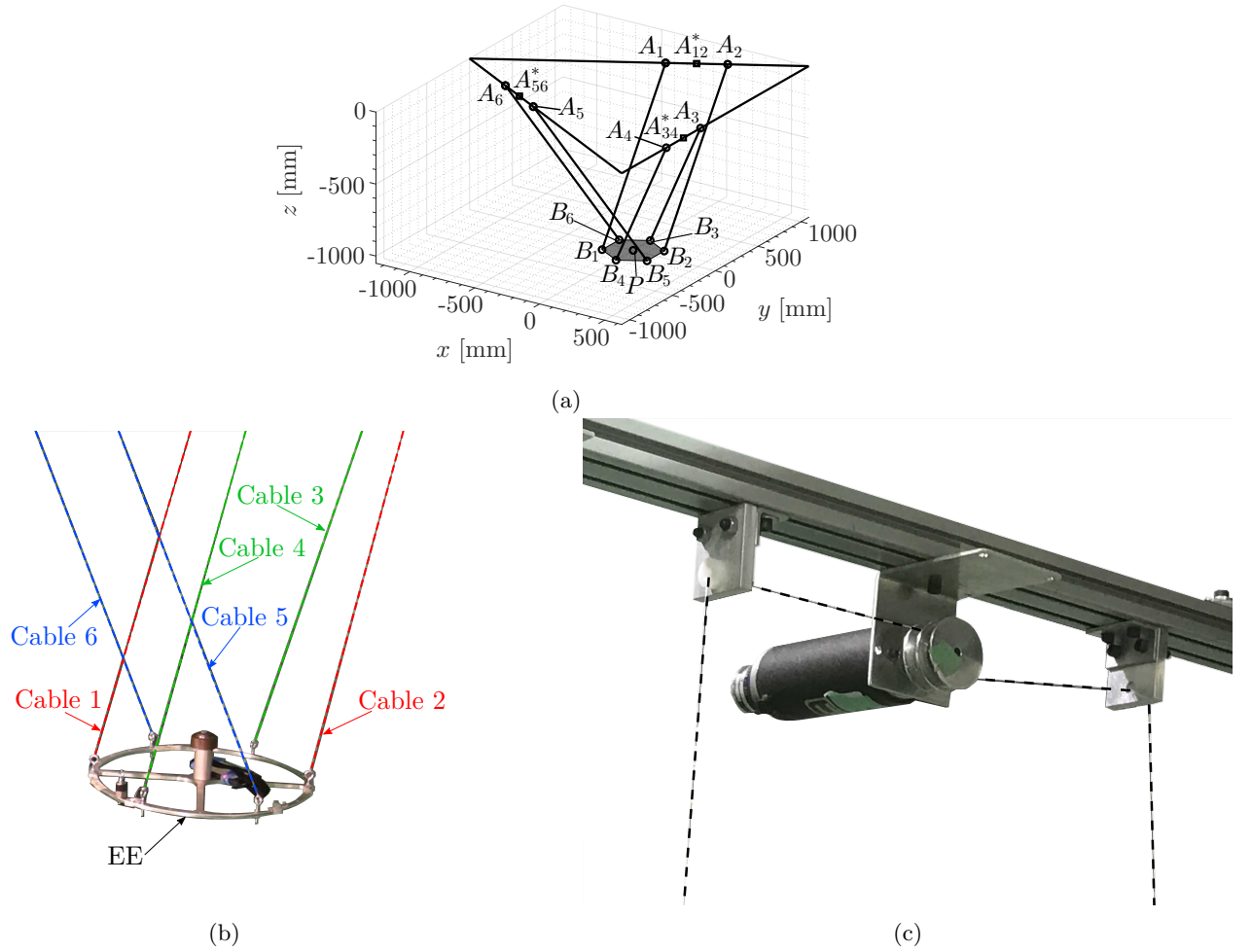
Figure 7: (a): a schematic of the prototype in the reference pose. The fixed frame $Oxyz$ has its origin in the plane of points A_i's, in the centre of the SEW. (b): top view of the prototype developed at Université Laval. (c): a photo of one of the robot winches, with two cables (highlighted by dashed lines) coiling on the same pulley.

The results can be seen in the attached video, showing the robot as it performs dynamic trajectories such as those presented in [5, 9]; the video shows the robot from two different viewpoints, one frontal and another above the robot. The robot is clearly moving outside the SEW (marked by a grey volume in the video) while keeping positive cable tensions and maintaining a constant orientation; also, it is easy to see that the cables remain parallel as the robot moves.

The video is divided in two parts:

- First, the robot performs a dynamic periodic trajectory such as those presented in [9]: the robot starts from rest and oscillates with increasing motion amplitudes until it moves along a horizontal circle centred in the centre of the SEW and having a radius larger than the workspace. After a few cycles, the robot is slowed down to its starting point (see Fig. 8a for a 3D plot of the trajectory).

- In the second part, we perform point-to-point dynamic motions reaching outside the SEW. At the target points the robot velocity is zero, but not the acceleration (the robot cannot be at rest out of the SEW); here, we used the method in [5] to plan the trajectories (see Fig. 8b).

The robot used for the tests is a prototype meant to be a proof of concept, thus not fully engineered. In any case, we verified that the desired trajectories were followed with an acceptable degree of accuracy, given the limitations of the prototype. We compared the desired position $\mathbf{p}_d$ along the motion with the estimated actual one $\mathbf{p}_e$: this is obtained by solving the forward kinematics with the real cable lengths $\rho_{i,e}$ as inputs (measured by the encoders on the robot motors). The plots of the norm of the difference $d\mathbf{p} = \mathbf{p}_e - \mathbf{p}_d$ between the desired and the actual periodic and point-to-point trajectories are shown in Figs. 8c and 8d, respectively. We found that the maximum positioning error during the periodic

---

[5]In this case, the two cables are either always crossing or never crossing, for any position of the robot.

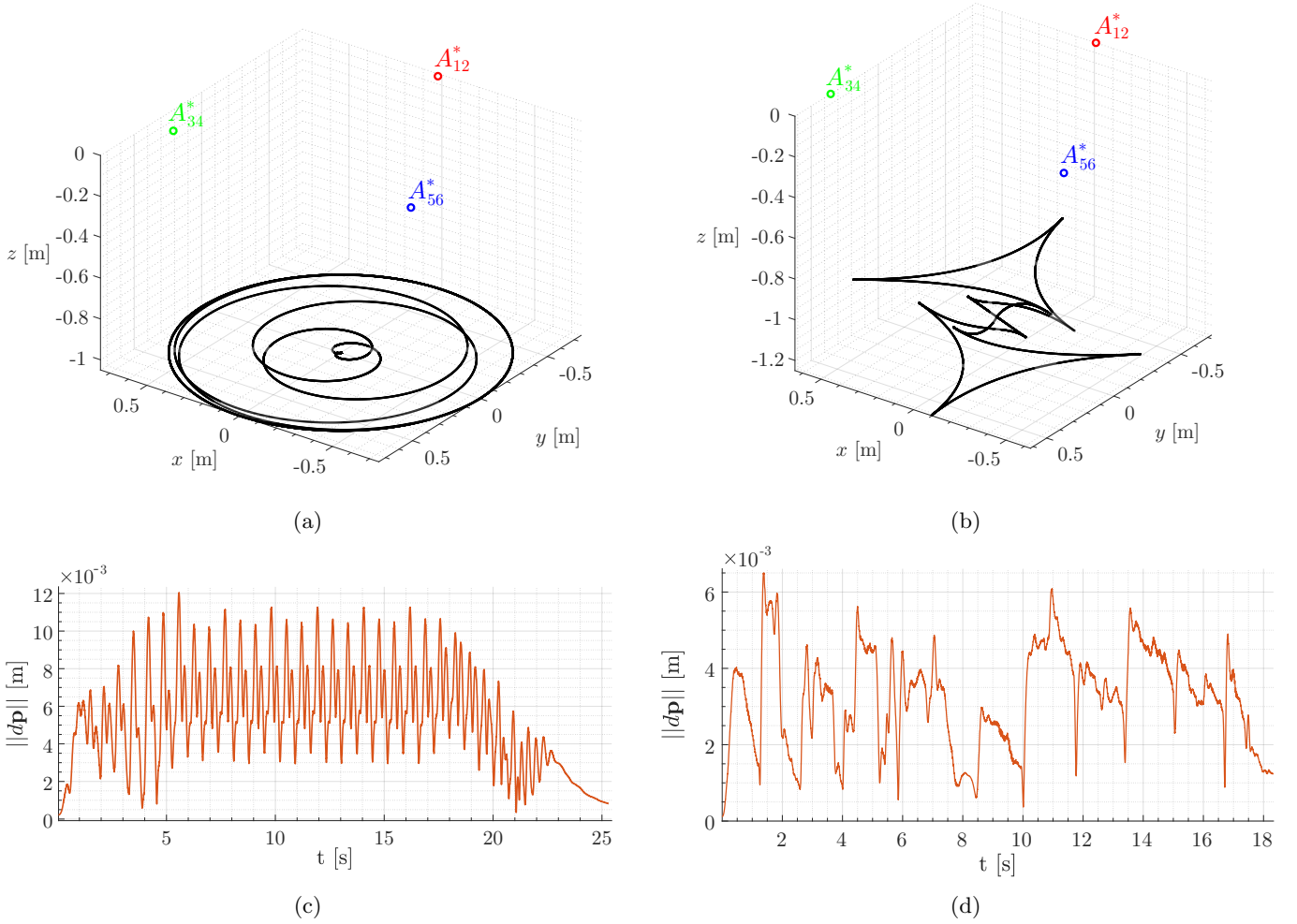[6]P does not have to be in the plane through points B_i's; if it is so, then $\Pi \equiv \Gamma$.

11

Figure 8: (a): 3D plot of the periodic motion. (b): 3D plot of the point-to-point motion. (c): plot of the position error $\|d\mathbf{p}\|$ along the periodic motion ($d\mathbf{p}$ is the distance between desired position $\mathbf{p}_d$ and the actual one $\mathbf{p}_e$). (d): plot of $\|d\mathbf{p}\|$ along the point-to-point motion.

motion was 1.205×10^{-2} m, with an average error of 5.36×10^{-3} m (respectively, 6.5×10^{-3} m and 3.2×10^{-3} m for the point-to-point motion). Considering the limitations of the prototype and that the robot was moving with high accelerations (up to $\sim 6.6\,\mathrm{m/s^2}$ during our tests) in a workspace that is meters wide, these errors can be considered to be acceptable.

To verify that the orientation was constant as the robot moved, we recorded the roll, pitch and yaw angles of the platform during the experiments by using the Inertial Measurement Unit (IMU) in a common smartphone that was secured on the robot platform. An example of the results can be seen in Fig. 9: the platform never rotated by more than 3° with respect its start pose, which seems an acceptable error given the approximations in the measurement of the architecture parameters. Such results are compatible with what was observed in [21], where the authors performed a multibody simulation of the dynamic behavior of a CSPR with a cable architecture similar to the one proposed here (except that the robot only moved in a vertical plane and employed eight cables, thus being overconstrained), observing a variation of the EE Euler angles not bigger than 1°. Given that in our case the accelerations are an order of magnitude higher and the robot moves outside its SEW, a larger orientation error is to be expected, also considering the very simple mechanical realization of the tested prototype. [7]

A potential issue of the special architecture defined in Sec. 4 is that it requires a careful design of the EE to ensure that its center of mass (CoM) is sufficiently close to the position of P, as an error in the estimation of the CoM location can produce an orientation error on the EE. Indeed, during some of our tests we did experience small orientation errors when the CoM was displaced from its nominal position in P; in any case, in the experiments presented in this paper the location of the CoM was accurately chosen in order to respect the condition in Sec. 4.

---

[7]Since a smartphone IMU is not a precision instrument (the RMS error on the orientation angles in dynamic conditions can be up to roughly 2° [49]), the results reported in Fig. 9 must not be intended as an accurate quantitative assessment of the orientation error. However, they provide a clear indication that the EE orientation remains reasonably constant.
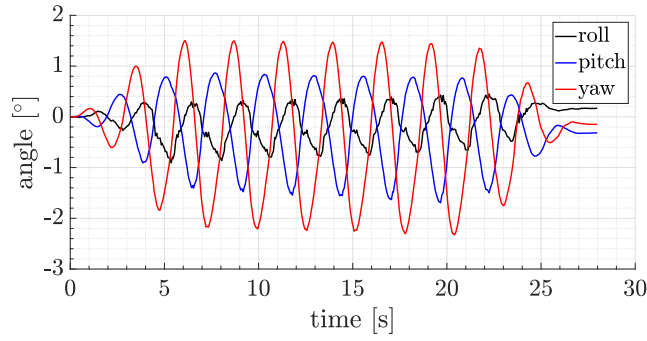
Figure 9: Yaw, pitch and roll angles of the robot, as measured by an IMU on the EE, with respect to the start position (where we set the three angles equal to zero) along a circular horizontal motion (see video).

8. Conclusions

In this paper, we investigated the properties of a general class of purely-translational cable-suspended parallel robots (CSPRs), with an end-effector (EE) of finite dimensions. We found that, under a rather general placement for the mobile cable attachment points, the robot can be modeled as a 3-cable CSPR with a point-mass EE. Under these conditions, the robot can be moved, while keeping a constant orientation of the EE, beyond its static workspace, by using the dynamic trajectories studied in [5, 9].

In order to perform dynamic trajectories feasible in practice, we also studied the singularity-free workspace, the reachable workspace, and the interference-free workspace, finding in all cases analytical formulations of the corresponding loci.

The robot at hand has vast motion capabilities and a stable behaviour during motion. Several special architectures were identified with distinctive and useful features.

The results from this paper combine ideas from previous works [9, 15] in a novel way.

Future plans include the study of the effect of control errors on the robot motion: since the translational properties of the CSPR under study assume that cables share pairwise the same length, we plan to study how orientation changes when small control errors are introduced. Also, the effect of the cable flexibility ought to be taken into account. Another possibility is to apply a gripper on the end-effector, as proposed in [18, 19]: given the high rotational stability that we observed in the experiments, the robot could be used to perform pick-and-place operations. As observed during experiments (Sec. 7), small errors in the EE's orientation can appear if the CoM's position is not accurately known; investigating sensitivity of the robot orientation to manufacturing errors with respect to the design parameters will be the object of future research. Finally, guaranteeing that maximum tensions are below a required threshold τ_{max} along a dynamic motion is left as future work.

9. Acknowledgments

References

[1] E. Stump, V. Kumar, Workspaces of cable-actuated parallel manipulators, ASME J. Mech. Des. 128 (1) (2006) 159–167. doi:10.1115/1.2121741.

[2] P. Bosscher, A. Riechel, I. Ebert-Uphoff, Wrench-feasible workspace generation for cable-driven robots, IEEE Trans. Robot. 22 (5) (2006) 890–902. doi:10.1109/TRO.2006.878967.

[3] D. Zanotto, G. Rosati, S. K. Agrawal, Modeling and control of a 3-DOF pendulum-like manipulator, in: Proc. of the 2011 IEEE Int. Conf. on Robotics and Automation, Shanghai, P.R.C., 2011, pp. 3964–3969. doi:10.1109/ICRA.2011.5980198.

[4] D. Cunningham, H. H. Asada, The Winch-Bot: A cable-suspended, under-actuated robot utilizing parametric self-excitation, in: Proc. of the 2009 IEEE Int. Conf. on Robotics and Automation, Kobe, Japan, 2009, pp. 1844–1850. doi:10.1109/ROBOT.2009.5152378.

[5] X. Jiang, C. Gosselin, Dynamic point-to-point trajectory planning of a three-DOF cable-suspended parallel robot, IEEE Trans. Robot. 32 (6) (2016) 1550–1557. `doi:10.1109/TRO.2016.2597315`.

[6] N. Zhang, W. Shang, Dynamic trajectory planning of a 3-DOF under-constrained cable-driven parallel robot, Mech. Mach. Theory 98 (2016) 21–35. `doi:10.1016/j.mechmachtheory.2015.11.007`.

[7] N. Zhang, W. Shang, S. Cong, Geometry-based trajectory planning of a 3-3 cable-suspended parallel robot, IEEE Trans. Robot. 33 (2) (2016) 484–491. `doi:10.1109/TRO.2016.2631591`.

[8] P. Dion-Gauvin, C. Gosselin, Trajectory planning for the static to dynamic transition of point-mass cable-suspended parallel mechanisms, Mech. Mach. Theory 113 (2017) 158–178. `doi:10.1016/j.mechmachtheory.2017.03.003`.

[9] G. Mottola, C. Gosselin, M. Carricato, Dynamically feasible periodic trajectories for generic spatial three-degree-of-freedom cable-suspended parallel robots, ASME J. Mech. Rob. 10 (3) (2018) 031004. `doi:10.1115/1.4039499`.

[10] N. Zhang, W. Shang, S. Cong, Dynamic trajectory planning for a spatial 3-DoF cable-suspended parallel robot, Mech. Mach. Theory 122 (2018) 177–196. `doi:10.1016/j.mechmachtheory.2017.12.023`.

[11] P. Dion-Gauvin, C. Gosselin, Dynamic point-to-point trajectory planning of a three-DOF cable-suspended mechanism using the hypocycloid curve, IEEE Trans. Mecha. 34 (3) (2018) 1–10. `doi:10.1109/TMECH.2018.2840051`.

[12] X. Jiang, E. Barnett, C. Gosselin, Dynamic point-to-point trajectory planning beyond the static workspace for six-DOF cable-suspended parallel robots, IEEE Trans. Robot. 34 (3) (2018) 1–13. `doi:10.1109/TRO.2018.2794549`.

[13] X. Jiang, E. Barnett, C. Gosselin, Periodic trajectory planning beyond the static workspace for 6-DOF cable-suspended parallel robots, IEEE Trans. Robot. 34 (3) (2018) 1–13. `doi:10.1109/TRO.2018.2819668`.

[14] Z. Shao, T. Li, X. Tang, L. Tang, H. Deng, Research on the dynamic trajectory of spatial cable-suspended parallel manipulators with actuation redundancy, Mechatronics 49 (2018) 26–35. `doi:10.1016/j.mechatronics.2017.11.001`.

[15] P. Bosscher, R. Williams, M. Tummino, A concept for rapidly-deployable cable robot search and rescue systems, in: Proc. of the ASME 2005 IDETC/CIE, Long Beach, USA, 2005, pp. 589–598. `doi:10.1115/DETC2005-84324`.

[16] P. Bosscher, R. Williams, L. Bryson, D. Castro-Lacouture, Cable-suspended robotic contour crafting system, Automation in construction 17 (1) (2007) 45–55. `doi:10.1016/j.autcon.2007.02.011`.

[17] R. Williams, M. Xin, P. Bosscher, Contour-crafting-cartesian-cable robot system: dynamics and controller design, in: Proc. of the ASME 2008 IDETC/CIE, New York, USA, 2008, pp. 39–45. `doi:10.1115/DETC2008-49480`.

[18] O. Saber, S. Abyaneh, H. Zohoor, A cable-suspended robot with a novel cable based end effector, in: Proc. of the ASME 2010 ESDA, Istanbul, Turkey, 2010, pp. 799–808. `doi:10.1115/ESDA2010-25312`.

[19] O. Saber, H. Zohoor, Workspace analysis of a cable-suspended robot with active-passive cables, in: Proc. of the ASME 2013 IDETC/CIE, Portland, USA, 2013. `doi:10.1115/DETC2013-12646`.

[20] E. Barnett, C. Gosselin, Large-scale 3D printing with a cable-suspended robot, Additive Manufacturing 7 (2015) 27–44. `doi:10.1016/j.addma.2015.05.001`.

[21] G. Castelli, E. Ottaviano, P. Rea, A Cartesian cable-suspended robot for improving end-users' mobility in an urban environment, Robotics and Computer-Integrated Manufacturing 30 (3) (2014) 335–343. `doi:10.1016/j.rcim.2013.11.001`.

[22] A. Alikhani, S. Behzadipour, S. Vanini, A. Alasty, Workspace analysis of a three DOF cable-driven mechanism, ASME J. Mech. Rob. 1 (4) (2009) 041005. `doi:10.1115/1.3204255`.

[23] A. Alikhani, S. Behzadipour, A. Alasty, S. Vanini, Design of a large-scale cable-driven robot with translational motion, Robotics and Computer-Integrated Manufacturing 27 (2) (2011) 357–366. `doi:10.1016/j.rcim.2010.07.019`.

[24] O. Saber, A spatial translational cable robot, ASME J. Mech. Rob. 7 (3) (2015) 031006. `doi:10.1115/1.4028287`.

[25] T. Le, H. Dobashi, K. Nagai, Kinematical and static force analysis on redundant drive wire mechanism with velocity constraint modules to reduce the number of actuators, Robomech 3 (1) (2016) 1–22. `doi:10.1186/s40648-016-0057-z`.

[26] S. Behzadipour, R. Dekker, A. Khajepour, E. Chan, DeltaBot: a new cable-based ultra high speed robot, in: Proc. of the ASME 2003 IMECE, Washington D.C., USA, 2003, pp. 533–537. `doi:10.1115/IMECE2003-41470`.

[27] S. Behzadipour, A. Khajepour, A new cable-based parallel robot with three degrees of freedom, Multibody System Dynamics 13 (4) (2005) 371–383. `doi:10.1007/s11044-005-3985-6`.

[28] S. Behzadipour, A. Khajepour, Cable-based robot manipulators with translational degrees of freedom, 2006, pp. 211–236. `doi:10.5772/5035`.

[29] Z. Zhang, Z. Shao, L. Wang, A. Shih, Optimal design of a high-speed pick-and-place cable-driven parallel robot, in: C. Gosselin, P. Cardou, T. Bruckmann, A. Pott (Eds.), Cable-Driven Parallel Robots, Springer, Québec, Canada, 2018, pp. 340–352. `doi:10.1007/978-3-319-61431-1_29`.

[30] D.-S. Vu, E. Barnett, A. Zaccarin, C. Gosselin, On the design of a three-DOF cable-suspended parallel robot based on a parallelogram arrangement of the cables, in: C. Gosselin, P. Cardou, T. Bruckmann, A. Pott (Eds.), Cable-Driven Parallel Robots, Springer, Québec, Canada, 2018, pp. 319–330. `doi:10.1007/978-3-319-61431-1_27`.

[31] A. Berti, J.-P. Merlet, M. Carricato, Solving the direct geometrico-static problem of underconstrained cable-driven parallel robots by interval analysis, Int. J. Robot. Research 35 (6) (2016) 723–739. `doi:10.1177/0278364915595277`.

[32] A. Berti, M. Gouttefarde, M. Carricato, Dynamic recovery of cable-suspended parallel robots after a cable failure, in: J. Lenarčič, J.-P. Merlet (Eds.), Advances in Robot Kinematics, Springer International Publishing, Grasse, France, 2016, pp. 337–344. `doi:10.1007/978-3-319-56802-7_35`.

[33] V. Schmidt, W. Kraus, W. Y. Ho, J. Seon, A. Pott, J. Park, A. Verl, Extending dynamic trajectories of cable-driven parallel robots as a novel robotic roller coaster, in: 41st Int. Symp. Robotics, Munich, Germany, Munich, Germany, 2014, pp. 367–373.

[34] M. Carricato, V. Parenti Castelli, On the topological and geometrical synthesis and classification of translational parallel mechanisms, in: 11th World Congress in Mechanism and Machine Science, Tianjin, China, 2004, pp. 1624–1628.

[35] A. T. Riechel, I. Ebert-Uphoff, Force-feasible workspace analysis for underconstrained point-mass cable robots, in: Proc. of the 2004 IEEE Int. Conf. on Robotics and Automation, New Orleans, USA, 2004, pp. 4956–4962. `doi:10.1109/ROBOT.2004.1302503`.

[36] J. Longval, C. Gosselin, Dynamic trajectory planning and geometric design of a two-DOF translational cable-suspended planar parallel robot using a parallelogram cable loop, in: Proc. of the ASME 2018 IDETC/CIE (in press), Québec, Canada, 2018, p. 10.

[37] D. Zlatanov, R. Fenton, B. Benhabib, A unifying framework for classification and interpretation of mechanism singularities, ASME J. Mech. Des. 117 (4) (1995) 566–572. `doi:10.1115/1.2826720`.

[38] M. Conconi, M. Carricato, A new assessment of singularities of parallel kinematic chains, IEEE Trans. Robot. 25 (4) (2009) 757–770. `doi:10.1109/TRO.2009.2020353`.

[39] B. M. St-Onge, C. Gosselin, Singularity analysis and representation of the general Gough-Stewart platform, Int. J. Rob. Res. 19 (3) (2000) 271–288. `doi:10.1177/02783640022066860`.

[40] R. D. Gregorio, V. Parenti Castelli, Mobility analysis of the 3-UPU parallel mechanism assembled for a pure translational motion, ASME J. Mech. Des. 124 (2) (2002) 259–264. `doi:10.1115/1.1471530`.

[41] V. Parenti Castelli, R. D. Gregorio, F. Bubani, Workspace and optimal design of a pure translation parallel manipulator, Meccanica 35 (3) (2000) 203–214. `doi:10.1023/A:1010359523780`.

[42] R. D. Gregorio, Determination of singularities in Delta-like manipulators, Int. J. Rob. Res. 23 (1) (2004) 89–96. `doi:10.1177/0278364904039689`.

[43] Y. Yang, W. Zhang, H. Pu, Y. Peng, A class of symmetrical 3T, 3T-1R, and 3R mechanisms with parallel linear motion elements, Journal of Mechanisms and Robotics 10 (5) (2018) 051016. `doi:10.1115/1.4040885`.

[44] M. Callegari, M. Tarantini, Kinematic analysis of a novel translational platform, ASME J. Mech. Des. 152 (2) (2003) 308–315. `doi:10.1115/1.1563637`.

[45] D. Hilbert, S. Cohn-Vossen, Geometry and the imagination, Chelsea Publishing Company, 1952.

[46] J.-P. Merlet, Analysis of the influence of wires interference on the workspace of wire robot, in: J. Lenarčič, C. Galletti (Eds.), On Advances in Robot Kinematics, Springer, 2004, pp. 211–218. `doi:10.1007/978-1-4020-2249-4_23`.

[47] S. Perreault, P. Cardou, C. Gosselin, M. Otis, Geometric determination of the interference-free constant-orientation workspace of parallel cable-driven mechanisms, ASME J. Mech. Rob. 2 (3) (2010) 031016. `doi:10.1115/1.4001780`.

[48] L. Blanchet, J.-P. Merlet, Interference detection for cable-driven parallel robots (CDPRs), in: 2014 IEEE/ASME Int. Conf. on Advanced Intelligent Mechatronics, Besançon, France, 2014, pp. 1413–1418. `doi:10.1109/AIM.2014.6878280`.

[49] Q. Mourcou, A. Fleury, C. Franco, F. Klopcic, N. Vuillerme, Performance evaluation of smartphone inertial sensors measurement for range of motion, Sensors 15 (9) (2015) 23168–23187. `doi:10.3390/s150923168`.